

Chang-Refsdal Microlensed Type Ia Supernova Light Curves

H. Bagherpour¹, B. Chen², R. Kantowski³, D. Branch⁴

*University of Oklahoma, Homer L. Dodge Department of Physics and Astronomy,
Norman, OK 73019, USA*

D. Richardson⁵

*Denison University, Department of Physics and Astronomy,
Granville, OH 43023, USA*

ABSTRACT

A description of the light curves of microlensed Type Ia supernovae (SNe Ia) as extended and expanding sources is presented. We give examples of what microlensing by stellar-mass Chang-Refsdal lenses can do to a small percentage of supernova light curves. We find that in addition to overall brightening, significant changes in light-curve shapes can also occur. Peaks can be distorted, plateaus can appear, and even secondary peaks can be formed. The effects of both the relative motion of the lens and the supernova and the expansion of the supernova are given and compared. The effects of relative motion are more pronounced when a distant supernova ($z_s \sim 1$) impacts well within the Einstein ring of a nearby microlens ($z_d \sim 0.05$) and are less important for more distant deflectors. We also find that the increase in shear that comes with increased deflector distance tends to reduce the time variability of microlensing. We briefly discuss the probability of observing these effects.

Subject headings: gravitational lensing — supernovae: general

¹hamed@nhn.ou.edu

²chen@nhn.ou.edu

³kantowski@nhn.ou.edu

⁴branch@nhn.ou.edu

⁵richardson@denison.edu

1. Introduction

Out of a number of distance indicators, Type Ia supernovae (SNe Ia) have emerged as the most promising standard candles. Due to their significant intrinsic brightness and relative ubiquity they can be observed in the local and distant universe. Several teams including the High- z Supernova Search (Schmidt et al. 1998) and the Supernova Cosmology Project (Perlmutter et al. 1999) have been searching for SNe Ia at higher redshifts since the early 1990’s. Light emitted from these ‘standard candles’ is subject to lensing by intervening objects while traversing the large distances involved (Kantowski, Vaughan, & Branch 1995); the further the light source, the higher its chance of being significantly lensed. In fact, for cosmologically distant sources, the probability is high that a distant point source will be ‘imaged’ (Press & Gunn 1973; Bourassa & Kantowski 1976; Wyithe & Turner 2002), particularly by stellar objects (microlensing). While the systematic errors introduced by K-correction, selection effects, and possible evolution can be removed, lensing might ultimately limit the accuracy of luminosity distance measurements (Perlmutter & Schmidt 2003). Only a large sample of SNe Ia at each redshift can be used to characterize the lensing distribution and to correct for the effect of weak lensing. Proposed searches, e.g., Tyson (2005); Corasaniti et al. (2006) are expected to yield hundreds of thousands of SNe Ia out to $z \sim 1$, some of which should exhibit lensing effects such as described here.

Properties of microlensed supernovae have been studied previously. Schneider & Wagoner (1987) presented the time-dependent amplification of supernovae caused by their expansion and showed that the related polarization is not likely to exceed 1% and hence not possible to detect among cosmologically distant supernovae at this time. Linder, Schneider, & Wagoner (1988) studied amplification of supernovae and developed approximate formulae for the amplification probability distribution. Rauch (1991) studied microlensing of SNe Ia by compact objects and calculated the resulting amplification probability distributions using Monte Carlo simulations. Assuming point-deflectors with shear Kolatt & Bartelmann (1998) estimated the microlensing rate by MACHOs in nearby clusters. The supernovae were treated as point sources and consequently the microlensed light curves were expected to contain amplification peaks similar to caustic crossing events seen in the OGLE data (Udalski 2003). In this paper, we demonstrate in detail how microlensing by a single stellar deflector in an external shear field can affect light curves of cosmologically distant SNe Ia. We use the lens model of Chang & Refsdal (1979) to calculate amplifications (Schneider, Ehlers & Falco 1992). We ignore any lensing amplification caused by the SN’s hosting galaxy and concentrate on the time-dependent effects caused by a single moving stellar deflector. We model the SNe Ia as expanding light sources with limb-darkening.

In the next section, we present our model for SNe Ia as microlensed sources. Section 3 is

devoted to a brief discussion of microlensing of finite-size sources, and in § 4 we present the results of our calculations. Throughout, we assume a flat Friedmann-Lemaître-Robertson-Walker cosmological model with $\Omega_m = 0.3$, $\Omega_\Lambda = 0.7$, and $h_{100} = 0.67$ to calculate the distances to the source and deflector.

2. Type Ia Supernovae

2.1. The Light Curve

To model the intrinsic SN Ia light curve we used a combination of two analytical models; that of Arnett (1982) for the peak of the light curve (the photospheric phase) and that of Jeffery (1999) for the tail (the nebular phase). The details of this model are in Richardson, Branch, & Baron (2005). The model parameters have been fixed for a typical SN Ia: the kinetic energy is 10^{51} erg), the total ejected mass is $1.4 M_\odot$, and the ^{56}Ni mass has been set to $0.6 M_\odot$. These values produce a peak absolute magnitude of $M_B = -19.5$ and a light-curve shape that conforms to the characteristic light-curve of normal SNe Ia, see the solid curves in the first rows of Figures 3-5.

2.2. The Radius

Because the effective size of a SN Ia varies with time and is on occasion of the same dimension as the lens caustics we need an expression for its time-dependent radius. For the photospheric phase ($t < 150$ days) we obtain the radius by multiplying the velocity at the photosphere of the homologously expanding ejecta, as determined empirically by Branch et al. (2005), by the time since explosion. For the nebular phase, we assume that the effective radius of the iron-group core expands at a constant velocity of 6000 km s^{-1} . A good fit for the velocity is then an exponential:

$$v(t) = 9.1 e^{(-t/36.5 \text{ days})} + 6.0, \quad (1)$$

in units of 10^3 km s^{-1} , from which the photospheric radius in AU is given by:

$$r_{SN}(t) = v(t) t = \left[5.3 e^{(-t/36.5 \text{ days})} + 3.5 \right] t. \quad (2)$$

Figure 1 shows the expansion velocity as well as the radius as a function of time.

2.3. Limb-darkening

For limb darkening in the nebular phase we assume uniform emissivity per unit volume (out to 6000 km s⁻¹) and find

$$I(r) = I_o \sqrt{1 - \left(\frac{r}{r_{SN}}\right)^2}, \quad (3)$$

where I_o is the intensity at the center and r_{SN} is the supernova's radius. The assumption of uniform emissivity per unit volume is a reasonable assumption during the nebular phase; to see whether the same expression can be used for the photospheric phase we compare it in Figure 2 to limb-darkening curves in the U and B bands calculated (courtesy of E. Lentz) for the W7 model (Nomoto, Thielemann, & Yokoi 1984). Considering that the detailed calculations are model dependent, the use of the simple nebular-phase expression for the photospheric phase is reasonable.

3. Microlensing of Extended Sources

3.1. Basics

The linearized Einstein theory for a static gravitational field gives a bending angle for light rays passing through a weak gravitational field of

$$\boldsymbol{\alpha} = -\frac{2}{c} \int_{-\infty}^{+\infty} \nabla \phi dt, \quad (4)$$

where ϕ is the Newtonian gravitational potential satisfying the boundary conditions $\phi \rightarrow 0$ at infinity, and where the integral is performed along the light path in the absence of the gravitational field. Bourassa, Kantowski, & Norton (1973), and Bourassa & Kantowski (1974, 1976) used the 2-component nature of $\boldsymbol{\alpha}$ to replace it with the complex scattering function $I(z)$, where $z = x + iy$ is the complex equivalent of the 2-d vector $\mathbf{r} = x\hat{i} + y\hat{j}$. Using $I(z)$, the relation between the source position, z , and image position, z_o , when both are projected onto the plane of the deflector is

$$z = z_o - \frac{4GD}{c^2} I^*(z_o), \quad (5)$$

where * means complex conjugate. The scaled (effective) distance D is defined as $D = D_{ds}D_d/D_s$, where the deflector-source distance, D_{ds} , the observer-deflector distance, D_d , and the observer-source distance, D_s , are all the same type distances, e.g., apparent size distances.

The effect of gravitational lensing on the apparent brightness of a distant source can be computed in various ways. For extended sources it is often easiest to employ the fact that the apparent brightness is proportional to the image’s apparent area, i.e., the brightness of a small source is amplified by a factor

$$A = \frac{\mathcal{A}_o}{\mathcal{A}}, \quad (6)$$

where \mathcal{A}_o is the area of the image and \mathcal{A} is the area of the source, both projected on the deflector plane.

3.1.1. The Schwarzschild Lens

In the case of an isolated point deflector, the scattering function takes a very simple form:

$$I(z_o) = \frac{m_d}{z_o}, \quad (7)$$

and the equation (5) reduces to

$$z = z_o - \frac{r_E^2}{z_o^*}, \quad (8)$$

where $r_E \equiv \sqrt{4Gm_d D c^{-2}} = \sqrt{2r_S D}$ is the Einstein ring radius, and r_S is the deflector’s Schwarzschild radius. This equation has two separate solutions (images) for any source position $r = |z|$,

$$r_{\pm} = |z_{\pm}| = \frac{1}{2} \left(\sqrt{r^2 + 4r_E^2} \pm r \right). \quad (9)$$

Both images are in line with source and deflector. The ‘primary’ image, r_+ , lies on the same side of the deflector while the ‘secondary’ image, r_- , is on the other side. In the case of microlensing, the angular separation of the two images is of the order of micro arcseconds and consequently seen as a single object. The Einstein ring occurs when source and deflector are aligned with the observer ($r = |z| = 0$) for which $r_+ = r_- = r_E$, and due to the symmetry of the lensing configuration the image is actually a ring.

For a point mass deflector and a small point-like source the combined amplification of the unresolved primary and secondary images as a function of the image positions r_{\pm} or the source position r is

$$A \equiv A_+ + A_- = \left| \frac{1}{1 - r_E^4/r_+^4} \right| + \left| \frac{1}{1 - r_E^4/r_-^4} \right| = \frac{r^2 + 2r_E^2}{r\sqrt{r^2 + 4r_E^2}}. \quad (10)$$

Measuring this amplification from a single observation is not possible since it is practically impossible to figure out the original source flux. However, if the luminosity of the source

varies with time in a predictable way as with SNe or if the source is of constant brightness and the lens is moving with respect to the line of sight to the source [as with observation of bulge stars; see, for instance, Sumi et al. (2004)], the amplification will change with time in a predictable way and it is possible to determine the amplification.

3.1.2. The Chang-Refsdal Lens

If a point mass lens is not isolated but instead lives in a gravity field which varies slowly on the length scale of r_E then the lens equation (8) changes to

$$z = z_o - \frac{r_E^2}{z_o^*} - \gamma z_o^* - \kappa z_o, \quad (11)$$

where γ is the complex shear and κ the convergence of the local gravity field (Witt 1990; Mao 1991). The convergence is proportional to the transparent surface mass density in the immediate neighborhood of the microlensing star and will be assumed to vanish in what we do here. The effects of a small convergence are easily accounted for and are not qualitatively different from $\kappa = 0$. Shear is introduced by the macro-lens structure of the galaxy as a whole as well as the nearby neighbors of the microlensing star, see Nityananda & Ostriker (1984); Totani (2002). It can introduce significant qualitative differences, e.g., if the source is within a 2-d domain bounded by the diamond shaped caustic ($|\gamma| < 1$, see rows 4 of Figures 3-5) there are 2 extra images not present with the isolated star. The two extra images exist because Eq. (11) has 4 solutions $z_o = z_1, z_2, z_3, z_4$ when the source z is inside the closed caustic curve and only 2 solutions when it is not. Expressions for the 4 (or 2) image positions equivalent to Eq. (9) exist (they are given by the 4 (or 2) real solutions of a quartic equation in $r_o^2 \equiv z_o z_o^*$) but are more complicated than Eq. (9). The expression for the amplification of each image is relatively simple when written as a function of the image's position z_o

$$A^{-1} = \left| (1 - \kappa)^2 - r_E^4/r_o^4 - \gamma\gamma^* + \gamma(r_E/z_o)^2 + \gamma^*(r_E/z_o^*)^2 \right|. \quad (12)$$

However, when written as a function of the source position z , A^{-1} is quite complicated and the equivalent of Eq. (10) is even worse. The critical curve (somewhat elliptically shaped when $\kappa + |\gamma| < 1$) for the Chang-Refsdal lens (equivalent to the circularly shaped Einstein ring for the Schwarzschild lens) is drawn by putting $A^{-1} \rightarrow 0$ in Eq. (12) and from that curve the diamond shaped caustic is drawn using Eq. (11), see row 4 of Figures 3-6. The minor-major axes for the critical curves and caustics are (in units of r_E) respectively $1/\sqrt{1 - \kappa \pm |\gamma|}$ and $2|\gamma|/\sqrt{1 - \kappa \pm |\gamma|}$ and are oriented along the x-y axes rotated counterclockwise through an angle of half the phase of γ .

3.2. Amplification of an Extended Source

If the source is not small, e.g., for the Schwarzschild lens, if r/r_E varies significantly across the source, differential amplification must be taken into account. In general to obtain the total flux received from an extended source, an integral of intensity I across the source may be required:

$$A = \frac{\int_{images} I d\mathcal{A}_o}{\int_{source} I d\mathcal{A}}. \quad (13)$$

If the surface brightness is constant across the source or if there is no differential amplification, the net amplification is simply given by equation (6) where \mathcal{A}_o can be any of the images areas or in fact the total image area (giving the total amplification).

3.2.1. The Schwarzschild Lens

The amplification of a disk source with constant surface brightness, lensed by an isolated point mass can be given analytically. If the circular extended source has a projected radius of a and is at a distance l from the center of a spherically symmetric deflector (a and l are measured in the deflector plane), the total area of the combined and unresolvable Schwarzschild images is

$$\mathcal{A}^{(total)} = \int_{-\frac{\pi}{2}}^{\frac{\pi}{2}} a (a + l \sin \varphi) \sqrt{1 + \frac{4r_E^2}{l^2 + a^2 + 2al \sin \varphi}} d\varphi \quad (14)$$

After a rather long calculation, the total amplification of a uniform disc is found to be

$$A_{disc}[a, l, r_E] = \eta \{ \mu_1 K(k) + \mu_2 E(k) + \mu_3 \Pi(n, k) \}, \quad (15)$$

(Witt & Mao 1994; Mao & Witt 1998) where K , E , and Π are respectively the first, second, and third complete elliptic integral with

$$k = \frac{16alr_E^2}{(l+a)^2((l-a)^2 + 4r_E^2)},$$

$$n = \frac{4al}{(a+l)^2},$$

and constants

$$\eta = \frac{1}{2\pi a^2 \sqrt{(l-a)^2 + 4r_E^2}},$$

$$\mu_1 = (l-a)(a^2 - l^2 - 8r_E^2),$$

$$\begin{aligned}\mu_2 &= (l + a) \left((l - a)^2 + 4r_E^2 \right) , \\ \mu_3 &= \frac{4(l - a)^2 (a^2 + r_E^2)}{l + a} .\end{aligned}$$

The above applies to the so called Schwarzschild lens where shear, γ , is negligible and the deflector’s size is sufficiently small.

The amplification of a thin ring of radius a can be computed using Eq. (10) as

$$A_{ring}(a, l, r_E) = \frac{1}{2\pi a} \frac{d}{da} \left[\pi a^2 A_{disc}(a, l, r_E) \right] , \quad (16)$$

and the net amplification for a limb-darkened source where photospheric radius is r_{ph} as

$$A_I(r_{ph}, l, r_E) = \frac{-\int_0^{r_{ph}} \frac{d}{da} [I(a)] \pi a^2 A_{disc}(a, l, r_E) da}{\int_0^{r_{ph}} I(a) 2\pi a da} . \quad (17)$$

For the intensity profile $I(r)$ given in Eq. (3), A_I simplifies to:

$$A_I(r_{ph}, l, r_E) = \frac{3}{2} \int_0^{\pi/2} \sin^3 \varphi A_{disc}[r_{ph} \sin \varphi, l, r_E] d\varphi , \quad (18)$$

where A_{disc} is the function introduced in Eq. (15).

3.2.2. The Chang-Refsdal Lens

For the Chang-Refsdal lens we resort to a Monte Carlo calculation, randomly covering the extended source with points and summing over each image amplification using Eq. (12) to compute the net amplification A . Even though Eq. (18) is valid for the Chang-Refsdal lens the absence of a known analytic expression for A_{disc} , good for arbitrary source sizes, prohibits its use. Schneider & Wagoner (1987) have given an analytic expression for the amplification of a small uniform disc near a long critical line, however, for moving and expanding SN sources this condition is short lived. The Monte Carlo calculation is easily adapted to account for an expanding and limb-darkened source and the $\gamma \rightarrow 0$ results agree with results from the above Schwarzschild lens. In most cases we were able to obtain accurate values for the amplification by using less than 100,000 points; however, we did have to eliminate noise from the Poisson statistics on occasion.

3.3. Probability

The relevant quantity in seeing a microlensing event is the optical depth τ . It is defined as the probability that a point source (or equivalently the center of an extended source) falls

inside the Einstein ring of some deflector. The brightness of a point source within r_E of a Schwarzschild lens is amplified by a factor of at least 1.34. For randomly located point deflectors the optical depth depends on the mass density of the deflectors and not on their number density (Press & Gunn 1973). Typical values of the optical depths for microlensing of nearby stellar sources are remarkably small. For instance, Sumi et al. (2003) gives an optical depth $\tau = 2.59_{-0.64}^{+0.84} \times 10^{-6}$ toward the Galactic Bulge (GB) in Baade’s window for events with time scales between 0.3 and 200 days. Because of the small value of τ , millions of stars need to be monitored when searching for microlensing in areas such as the GB or the Large and Small Magellanic Clouds. The value of τ is much higher for cosmologically distant sources.

If we look at bulge-bulge lensing, Han & Gould (2003) give a model for the bulge from which a value of $\tau = 0.98 \times 10^{-6}$ is computed. They additionally compute an effective column density for deflectors $\Sigma_* = 2086 \text{ M}_\odot \text{pc}^{-2}$ and a characteristic source-lens separation $\overline{D} = 782 \text{ pc}$ defined by

$$\tau = \frac{4\pi G}{c^2} \Sigma_* \overline{D}. \quad (19)$$

If we now look at the bulge of a similar galaxy at $z = 0.05$ we expect a similar Σ_* but \overline{D} becomes the distance to the deflector D_d and hence increased by a factor $\approx 2.7 \times 10^5$. This would bring the optical depth up to 27% when looking through such a galaxy. At this distance the size of the bulge is ~ 1 arcsec and clearly resolvable. The downside is one of alignment. What is the chance of a galaxy hosting a SN being appropriately aligned with a foreground galaxy? The best place to see this effect seems to be the foregrounds of dense clusters. Because the SN Ia rate in the typical galaxy at $z = 1$ is about one per hundred years, some $370(1 + z)$ alignments would have to be followed for a year to see one event.

Besides the work of Rauch (1991) and Kolatt & Bartelmann (1998) mentioned earlier, others have made detailed estimates of micro-lensing probabilities. Assuming that the ordinary stellar populations of galaxies are the dominant causes of microlensing events, Wyithe & Turner (2002) concluded that in a flat universe, at least 1% of high-redshift sources ($z_s \geq 1$) are microlensed by stars at any given time. Zakharov, Popović, & Jovanović (2004) estimated that the optical depth for microlensing caused by deflectors both localized in galaxies and distributed uniformly, might reach 10% for sources at $z_s \sim 2$. Assuming low mass Chang-RRefsdal deflectors Kolatt & Bartelmann (1998) estimated that the microlensing rate of SNe by MACHOs in nearby clusters ($z \leq 0.05$) would be $\sim 0.02(f/0.01)$ per year where f is the fraction of the cluster mass in MACHOs ($10^{-7} \leq M_{macho}/M_\odot < 10^{-4}$).

As mentioned above, the amplification of a point source falling inside the Einstein ring r_E of a Schwarzschild lens is larger than 1.34. The probability of a larger amplification is proportionally smaller, e.g., the probability of having an amplification larger than A for a

given lensing configuration is

$$p(A) = u_A^2 \tau(z_s), \quad (20)$$

where $u_A \equiv b_A/r_E$ is the normalized impact parameter, that results in amplification A (Paczynski 1986a,b) and $\tau(z_s)$ is the optical depth for a source at redshift z_s . For a point source, the result is

$$u_A = \sqrt{2 \left(\frac{A}{\sqrt{A^2 - 1}} - 1 \right)}. \quad (21)$$

The standard optical depth τ significantly overestimates the probability that the interesting cases discussed in § 4 will occur. Using Eq.(20) or Eq.(21) we can try to correct for the overestimate. For these lensing configurations, the normalized impact parameter u_A does not exceed 0.1 ($A \approx 9$ for the point source) which gives a maximum probability of $\sim 10^{-4}$ for $z_s \geq 1$ ($\tau = 0.01$) if Wyithe & Turner (2002) are correct, and $\sim 10^{-3}$ for $z_s = 2$ ($\tau = 0.1$) if Zakharov, Popović, & Jovanović (2004) are correct. These numbers above are somewhat higher than Linder, Schneider, & Wagoner (1988) were predicting for Type I SN but not for Type II. Probabilities likes these, together with time scales of some cases studied here, imply that such effects may not be observed unless a large number of cosmologically distant (around 10^4 for $z_s \geq 1$) SNe Ia are followed for a period of up to 2 years.

Numerous probability estimates for weak (single-image) and strong (multi-image) macrolensing of supernova have been made for possible deep searches (Wang 2000; Holz 2001; Goobar 2002; Amanullah 2003). Oguri, Suto, & Turner (2003) summarizes that 0.05-0.1 % of the SN observed by SNAP at $z \sim 1$ would be macro-lensed. Such estimates can be used to indicate micro-lensing probabilities because a significant number of the deflectors for such observations would be at $z_d \approx 0.35$ and hence at high optical depth for micro-lensing. Large amplifications can also cause a bias in favor of observing supernovae, allowing one to observe more distant objects, and as a result, to increase the depth of any supernova survey. Gunnarsson & Goobar (2003) estimate that huge increases (e.g., 100%) in observable SN to 27th magnitude could occur if one simply searches in the direction of large clusters.

For the high amplification cases seen in the next section where the micro-lensed light-curves have a second peak, a separate probability estimate, consistent with the above, is given in the Appendix.

4. Microlensed Light Curves

In this section we use the SN Ia model of § 2 and the microlensing theory of § 3 to predict the shape of lensed light curves of SNe Ia for moving lenses. We have calculated

absolute magnitudes of the lensed light curves in the V-band. We concentrate on sources at redshifts $z_s = 1.0$ which are lensed by Chang-Refsdal deflectors at redshifts $z_d = 0.05, 0.10,$ and 0.35 . We use $z_d = 0.35$ because most lensing is expected to occur at this redshift, i.e., $D = D_d D_{ds} / D_s$ is \sim maximum. To calculate the amplification as a function of time we need to know the distance $l(t)$ between the supernova’s center and the deflector, projected on the plane of the deflector,

$$l(t) = \sqrt{l_o^2 + vt \left(vt \mp 2\sqrt{l_o^2 - b^2} \right)}, \quad (22)$$

where the minus sign is used when the supernova source explodes ($t = 0$ and $l = l_o$) before getting to the point of closest approach, b , and the plus sign when it explodes after. We also need the time dependent supernova’s radius Eq.(2), and the limb-darkening expression Eq.(3), both projected onto the deflector’s plane. The time in Eq.(22) is deflector time t_d whereas the time in Eq.(2) is source time $t_s = (1 + z_d)/(1 + z_s) t_d$ and both must be appropriately redshifted to be displayed in observer time as in Figures 3-5. When the shear vanishes we used the Schwarzschild lens result Eq.(18), and when $\gamma \neq 0$ we resorted to a Monte-Carlo procedure as indicated in §3.2.2. Because γ is orientation dependent, microlensing depends on both its magnitude and direction, see Eq. (11). However, the resulting amplification Eq. (12) is sensitive to orientation mainly when the projected photosphere is smaller than the caustic’s dimension. We are able to give a representative sample of SN lensing by aligning the caustic with the y -axis and having the deflector move parallel to the x -axis.

We plot light curves for various values of the parameters m_d, b, l_o, v (the relative speed of source and deflector projected on the deflector’s plane) and $|\gamma|$ (the magnitude of the shear caused by the deflector’s neighbors and/or the galaxy as a whole). Our sample deflector masses are $10^{-3} M_\odot, 1 M_\odot,$ and $10 M_\odot$. We fix the origin on the deflector and take the source to move in the deflector plane for 1,000 days (observer time) with three relative projected speeds of the source $v, 0.1 \text{ AU/day}, 0.5 \text{ AU/day},$ and $1.0 \text{ AU/day} = 1,730 \text{ km/sec}$.

Figures 3 through 5 show the light curves (1st row of panels) and the amplification curves (2nd row of panels) for lensed $z_s = 1$ supernovae with a total of six different configurations of moving deflectors at $z_d = 0.05$. The abscissas for the first 3 rows are in days since explosion. Each figure is for a fixed mass and contains two lensing configurations (left and right columns). Each panel of the first 2 rows show curves corresponding to 3 values of shear ($\gamma = 0$ i.e., the Schwarzschild lens, and two values of $\gamma \neq 0$ i.e., the Chang-Refsdal lens). These interesting cases have been selected from a number of configurations. Each panel in the 3rd row contains six curves of magnitude differences and show the relative importance of the deflector-lens motion versus photospheric expansion as a function of redshift. We have plotted the lensed magnitudes with relative transverse deflector motion minus lensed

magnitudes without motion for two lenses at three redshifts, $z_d = 0.05, 0.10,$ and 0.35 . Because the local shear of a given macro-lens varies with deflector distance z_d , we have appropriately varied γ in the 3rd row. The two starting values of γ are zero and one of the two values in the first 2 rows (either $\gamma = 0.20$ or 0.15) where $z_d = 0.05$. At $z_d = 0.10$ and 0.35 , γ is scaled by 1.76 and 3.15 respectively. In the 4th row of 4 panels we show the deflector plane position and size (in units of r_E) of the moving supernova’s photosphere relative to the caustics at two or three different times: 1 day after explosion (only shown in Figure 3), at the time of maximum light (20 days in the SN’s restframe), and at the time T_b the SN’s center reaches minimum impact at $r = b$. Because of the scale in Figures 4 and 6, the supernova’s position and size at 1 day don’t appear to be much different than at 20 days and hence are not shown. For both lensing configurations (left and right columns) row 4 contains 2 panels (left and right) which show the circular photospheres at the two deflector redshifts, $z_d = 0.05$ and $z_d = 0.35$ respectively. The $z_d = 0.05$ panels show the diamond shaped caustics for the two non-zero shears of rows 1 and 2 and the $z_d = 0.35$ panels show the caustic for the $\gamma \neq 0$ value used in row 3. If the caustic for the smaller shear is too small to distinguish from a point at the origin it is not shown.

We are plotting amplified absolute magnitudes of the supernova in the V-band, however, due to the redshift of the source, these light curves would be observed in the I-band. With the source located at $z_s = 1$, $M_V > -15.5$ is too dim to be seen. Nonetheless, we include the complete amplification and light curves to show their trends over a period of 1,000 observer days after the supernova explosion. It should be noticed that amplification curves are not symmetric (like those of point sources) because of the photosphere’s expansion.

For many cases, microlensing has a less than dramatic effect on the light curve’s shape; it simply provides an overall increase in its magnitude, and would be difficult to distinguish from amplification due to the galaxy or cluster hosting the lens, see Saini, Raychaudhury, & Shchekinov (2000). However in more interesting cases, we can easily match the features in the light curve to the corresponding features in the amplification curve.

Figure 3 configurations both show an overall amplification around the supernova’s peak brightness as well as a discernible distortion in the peak itself as a result of a narrow-width rise in the amplification at this early time (see the inserts in row 1). For example, in our model light curve (§2.1) the ΔM_{20} parameter, the decline in magnitudes of the V–band light curve during the first 20 days after maximum light, is 1.10. This value (in the SN rest frame) is increased to 1.33, 1.17, and 1.23 for the respective values of shear $\gamma = 0, 0.20,$ and 0.40 shown in the left column of Figure 3, and to 1.57, 1.46, and 1.22 for the configuration of the right column. These changes in ΔM_{20} are rather large. After the peak phase, shear has little effect on the remainder of the light curve for either configuration.

When the photosphere is small compared to the caustic structure, high amplification is possible from a neighboring caustic, (e.g., see the $\gamma = 0.2$ caustic at $z_d = 0.05$ of the left panel of the left column or row 4), however, the intrinsic brightness of the SN is undetectably low then. When the SN is near its peak brightness, the photosphere has grown to be the size of the caustic structure and the amplification is maximum; continued expansion then reduces the net amplification. The third row is the result of computing lensed light curves without relative motion and subtracting them from light curves similar to those in the first row, i.e., lensed light curves where the relative motion is present. The right column of row 3 shows that relative motion effects can be distinguished from photospheric expansion in some cases, e.g., a full magnitude difference can occur at $z_d = 0.05$ when relative motion is included. As expected the magnitude differences diminish with redshift and are practically gone when $z_d = 0.35$. The photosphere’s expansion speed, when projected into the deflector plane, increases with deflector redshift and becomes more important whereas the deflector’s relative transverse speed would be roughly constant for real lenses (exactly constant for our examples). The second and fourth panels of the fourth row show why shear and relative motion become less important with increasing redshift, i.e., the photosphere is even larger relative to the caustic structure and motion produces smaller relative displacements.

The larger mass deflectors of Figures 4 and 5 have larger Einstein ring sizes and hence larger caustic dimensions relative to SN displacements and photosphere sizes at any given time. For these cases the amplification is larger and shear can change the amplification curves significantly; however, Schwarzschild deflectors often produce amplification peaks larger than Chang-Refsdal deflectors as is seen in Fig. 4 and in the left column of Fig. 5.

These more massive lenses show a large overall increase in the brightness of the whole light curve together with occasional second maxima occurring much later than the peak brightness. A low shear seems more likely to produce a plateau or a second peak, however, the reverse is the case for the configuration shown in the right column of Figure 5. For this configuration $v = 1.0$ AU/day = 1,730 km/sec is large enough to have the photosphere cross a caustic while its size remains smaller than the caustic dimension. The second caustic crossing would appear beyond 1000 days. In the left column where $v = 0.5$ AU/day the $\gamma = 0.05$ caustic is crossed before 100 days, which alters the SN’s peak brightness, but then significant photospheric expansion occurs before reaching the second caustic and results in a long flat amplification curve. Likewise, for the left column, 2nd row, $\gamma = 0.05$ case of Figure 4 a caustic crossing peak in amplification occurs early and distorts the magnitude peak. The source is small when it crosses the caustic after which expansion occurs rapidly causing little more than a rise in the remainder of the light curve.

Whether or not a second peak occurs in the light curve depends on the height and width

of the net amplification peak and when it occurs in the life of the SN. In general we can say that for small shear the presence of a peak in the amplification curve occurs around the time of minimum impact, however, for larger shears, caustic crossings distort the amplification peak towards the caustic crossing times as seen in Figures 4 and 5. If the caustic crossings coincide with minimum impact as in the right column of Fig. 5 when $z_d = 0.05$ and $\gamma = 0.10$, the total amplification is much enhanced. At lower speeds the amplification curves flatten out and remove any possibility of a second peak occurring in the light curve. For example the plateaus in the $\gamma = 0$ curves of row 1 of Figure 4 are still present (but diminished) at $z_d = 0.10$ and are gone by $z_d = 0.35$. For higher redshift deflectors, relative motion diminishes relative to the increased caustic size and photospheric expansion levels the amplification curve.

5. Conclusion

We have shown that microlensing can significantly affect light curves of some cosmologically distant SNe Ia. We restricted our calculation to sources at $z_s = 1$ in the currently accepted $\Omega_m = 0.3$, $\Omega_\Lambda = 0.7$ flat cosmological model. We found that microlensing can not only increase the magnitude of the light curve but also can cause a change in its shape. Relative transverse motion of the SN and lens, when added to the expanding photosphere, can result in features such as an enhanced peak brightness with a distorted shape as in Figure 3, a post peak plateau as in Figure 4, or even the presence of a wide second peak as in Figure 5.

In the absence of relative lens-source motion Schneider & Wagoner (1987) found distortions to the light curve’s peak caused by the supernova’s photosphere expanding into a deflector’s critical point as well as into its caustics. However, from row 3 of Figures 3-5 it is easy to see how ignoring the relative motion at small deflector redshifts can result in underestimating the variety and intensity of lensing effects on the SNe light curves. We find that stationary deflectors do not produce features such as bumps or plateaus as often as the corresponding moving deflectors. This is due to the fact that the amplification curves for stationary lenses tend to be flattened and show less change in amplification as the photosphere expands through and beyond the deflector. The effect of amplification by stationary deflectors appears to produce more of an overall upward shift in the supernova’s light curve. A look at row 3 of Figures 3 through 5 shows that the magnitude difference of the moving versus stationary cases is measurable for the deflectors at $z_d=0.05$ and 0.10 but not as far as 0.35 . The magnitude differences fall below 0.1 at $z \sim 0.25$.

Also, it should be pointed out that a supernova lensed by a stationary deflector is brighter than one lensed by a moving deflector beyond the time when the projected distance

of source and deflector is greater than the initial value l_o ; see, for instance, the right column of row 3 of Figure 3 where the two $z_d = 0.05$ curves go negative at $T = 169$ days.

In § 3 we pointed out, that for microlensing by compact masses distributed through the cosmos, the optical depth is 0.01 ($z_s \sim 1$) and might reach 0.1 ($z_s \sim 2$), implying that the overall chance of a distant SN Ia being microlensed is not negligible. Any multi-band supernova survey aimed at finding supernovae at redshifts around $z = 1$ (and above), could discover and identify *one* microlensed SN Ia event out of roughly *a hundred* events. However, the low impact parameters required to produce the special features depicted in § 4 demand observation of $\sim 10^4$ supernovae at $z_s \geq 1$. To see unusual features such as double peaks, the lensed supernova must be followed for an extended period of ~ 2 years. In the Appendix we have made an optical-depth type estimate to include double peak events. For microlensing by stars in the bulge of a galaxy at $z_d = 0.05$ we find a max probability of $\sim 1.7 \times 10^{-3}$. This is an ideal deflector distance for observing double peaks due to transverse motion. As expected this number is only slightly smaller than the 27% optical depth estimate made in §3.3 for bulge lensing when corrected for an impact parameter of $u = 0.1$. These estimates can double when the observational bias in favor of amplified events are taken advantage of (see, for instance, Gunnarsson & Goobar (2003)). It is interesting to note that according to OGLE III (Udalski 2003) a histogram of u values for Bulge lensing peaks at $u \sim 0.1$, probably due to amplification biasing.

Notice that we have not taken into account macrolensing convergence effects caused by the deflector’s host galaxy. The effects of convergence are relatively easy to include, e.g., in our case the amplifications for the Schwarzschild lens given in the second rows of Figure 3-5 would increase by $\sim 30\%$ if the lens galaxy had an unexpectedly high transparent surface mass density of $\Sigma = 1000 \text{ M}_\odot \text{pc}^{-2}$ at the image.

The authors are pleased to thank Eric Lentz for providing the limb-darkening curves for model W7 and Zach Blankenship for correcting an oversight in our work. This work was in part supported by NSF grants AST-0204771 and AST-0506028, and NASA grants NNG04GD36G NAG5-3505.

A. Appendix

In this appendix we compute the probability that a source, followed for a period T , impacts a Schwarzschild lens with a reduced impact parameter less than $u \equiv b/r_E$ and simultaneously moves at least a distance b during the period T . Such a time dependent impact will cause a change in the amplification of 10%-50% depending on the actual impact.

The idea here is to estimate the chance of seeing a distortion in the light curve of a SN whose life time is $T_{SN} \sim 200$ days.

We start with a number density N_d of mass m deflectors (located at a distance D_d from the observer) moving with relative transverse velocities distributed according to:

$$\frac{dN_d}{dv} = N_d(D_d) \frac{v}{v_{rms}^2} e^{-v^2/2v_{rms}^2}. \quad (\text{A1})$$

The probability of one of these moving deflectors impacting the line of sight to a source at D_s with a reduced impact parameter $\leq u$ and moving a reduced distance $\geq u$ during a period T is:

$$\Delta Prob(u, T) = \int_0^{D_s} dD_d \int_{ur_E/T}^{\infty} dv N_d(D_d) (\pi u^2 r_E^2 + 2ur_E v T) \frac{v}{v_{rms}^2} e^{-v^2/2v_{rms}^2}. \quad (\text{A2})$$

The integrand is the sum over cigar-shaped areas with widths $2ur_E$ and lengths $vT_{SN} + 2ur_E$ (traced out by the moving deflectors). The velocity integral can be done easily, and if the deflectors are effectively confined to a plane, the result can be written as

$$\Delta Prob(u, \xi) = \frac{4G}{c^2} \Sigma D u^2 \left\{ (\pi + 2) e^{-\xi^2/2} + \sqrt{2\pi} \frac{Erfc(\xi/\sqrt{2})}{\xi} \right\}, \quad (\text{A3})$$

where

$$\xi \equiv \frac{ur_E}{v_{rms}T} = u \frac{T_{rms}}{T}, \quad (\text{A4})$$

Σ is the projected surface mass density

$$\Sigma \equiv \int_0^{D_s} m N_d(D_d) dD_d, \quad (\text{A5})$$

and $Erfc$ is an error function.

The characteristic crossing time for microlensing is defined by $T_{rms} = r_E/v_{rms} = \sqrt{2r_S D}/v_{rms}$ (see § 3 for definitions) which for Galaxy bulge-bulge lensing is about 10 days (Udalski 2003). For a similar galaxy at redshift $z = 0.05$ lensing a distant SN through its bulge, the reduced distance D is increased by a factor of $\sim 2.7 \times 10^5$ [see § 3.3 and Han & Gould (2003)] and hence T_{rms} increases to $\sim 5,200$ days. If $u \sim 0.05$ and $T = T_{SN} \sim 200$ days, then $\xi \sim 1.3$ and $\Delta Prob(0.05, 1.3) \sim 1.7 \times 10^{-3}$. This particular probability falls off by at least an order of magnitude when $u < 0.01$ or $u > 0.15$.

REFERENCES

- Amanullah, R., Mrtzell, E., & Goobar, A. 2003, *A&A*, 397, 819
- Arnett, D. 1982, *ApJ*, 253, 785
- Arnett, D. 1996, *Supernovae and Nucleosynthesis* (Princeton: Princeton University Press)
- Branch, D., et al. 2005, *PASP*, 117, 545
- Bourassa, R. R., Kantowski, R., & Norton T. D. 1973, *ApJ*, 185, 747
- Bourassa, R. R., & kantowski, R. 1974, *ApJ*, 195, 13
- Bourassa, R. R., & kantowski, R. 1976, *ApJ*, 205, 674
- Chang, K., & Refsdal, S. 1979, *Nature*, 282, 561
- Corasaniti, P. S., LoVerde, M., Crofts, A., & Blake, C. 2006, *MNRAS*, 369, 798
- Goobar, A., Mrtzell, E., Amanullah, R., Nugent, P. 2002, *A&A*, 393, 25
- Gunnarsson, C., & Goobar, A. 2003, *A&A*, 405, 859
- Han, C., & Gould, A. 2003, *ApJ*, 592, 172
- Holz, D. E. 2001, *ApJ*, 556, L71
- Jeffery, D. 1999, *astro-ph/9907015*
- Kantowski, R., Vaughan, T., & Branch, D. 1995, *ApJ*, 447, 35
- Kolatt, T. S., & Bartelmann, M. 1998, *MNRAS*, 296, 763
- Linder, E., Schneider, P., & Wagoner, R. V. 1988, *ApJ*, 324, 786
- Mao, S. 1991, *ApJ*, 389, 63
- Mao, S., & Witt, H. J. 1998, *MNRAS*, 300, 1041
- Nomoto, K., Thielemann, F., & Yokoi, K. 1984, *ApJ*, 286, 644
- Nityananda, R., & Ostriker, J. P. 1984, *J. Astrophys. Astr.*, 5, 235
- Oguri, M., Suto, Y., & Turner, E. L. 2003, *ApJ*, 583, 584
- Paczynski, B. 1986a, *ApJ*, 301, 503

- Paczynski, B. 1986b, *ApJ*, 304, 1
- Perlmutter, S., et al. 1999, *ApJ*, 517, 565
- Perlmutter, S., & Schmidt B. P. 2003, *Lecture Notes in Physics*, ed. K. Weiler (Berlin: Springer-Verlag)
- Press, W. H., & Gunn, J. E. 1973, *ApJ*, 185, 397
- Rauch, K. P. 1991, *ApJ*, 374, 83
- Richardson, D., Branch, D., & Baron, E. 2006, *AJ*, 131, 2233
- Riess, A., Press, W. H., & Kirshner, R. P. 1995, *ApJ*, 438, L17
- Saini, T. D., Raychaudhury, S., & Shchekinov, Y. A. 2000, *A&A*, 363, 349
- Schmidt, B. P., et al. 1998, *ApJ*, 507, 46
- Schneider, P., & Wagoner, R. V. 1987, *ApJ*, 314, 154
- Schneider, P., Ehlers, J., & Falco, E. E. 1992, *Gravitational Lenses* (Berlin:Spinger)
- Sumi, T., et al. 2003, *ApJ*, 591, 204
- Sumi, T., et al. 2004, *MNRAS*, 348, 1439
- Totani, T. 2003, *ApJ*, 586, 735
- Tyson, J. 2005, in *Observing Dark Energy*, ed. S. C. Wolff & T. Lauer (San Francisco; ASP), 95
- Udalski, A. 2003, *Acta Astron.*, 53, 291 (data taken from NOOS & EWS of OGLE III, <http://www.astrouw.edu.pl/~ogle/>)
- Wang, Y. 2000, *ApJ*, 531, 676
- Witt, H. J. 1990, *A&A*, 236, 311
- Witt, H. J., & Mao, S. 1994, *ApJ*, 430, 505
- Wyithe, J. S. B., & Turner, E. L. 2002, *ApJ*, 567, 18
- Zakharov, A. F., Popović, L. Č., & Jovanović, P. 2004, *A&A*, 420, 881

Fig. 1.—

Expansion velocity in km s^{-1} (*left axis*: filled triangles are observed data and dotted curve is an exponential fit) and the radius in AU (*right axis*: solid curve assuming homologous expansion) are plotted against time since explosion.

Fig. 2.—

Normalized limb-darkening curves in the U and B bands calculated for the W7 model at 15 days after explosion, and two curves $\propto \sqrt{1 - r^2/r_{SN}^2}$ for homologous expansion velocities of $13,000 \text{ km s}^{-1}$ and $15,000 \text{ km s}^{-1}$.

Fig. 3.—

Light curves (*1st row*) and amplification curves (*2nd row*) of a SN Ia at $z_s = 1.0$, microlensed by a deflector at $z_d = 0.05$ with a mass of $m_d = 10^{-3} M_\odot$ for two different relative transverse velocities $\mathbf{v} = v \hat{i}$, impact positions $\mathbf{b} = b \hat{j}$, and initial distances l_0 (left and right Columns). The un-lensed lightcurve is the solid line in the *1st row*. In the *3rd row* the difference in lensed light curves, caused by moving minus non-moving deflectors, are shown for $\gamma = 0$ at three redshifts $z_d = 0.05, 0.10$ and 0.35 , and for three shears $\gamma = 0.20, 0.35 (= 1.76 \times 0.20), 0.63 (= 3.15 \times 0.20)$ at the same three respective redshifts. Larger z_d 's are plotted with thicker lines, $\gamma = 0$ as dotted curves and the largest γ as dashed curves. When a given microlens and its environment is taken from $z = 0.05$ and placed at 0.10 and 0.35 , γ scales as 1.76 and 3.15 respectively ($\propto D \equiv D_d D_{ds} / D_s$). The *4th row* shows the position and size of the moving supernova's photosphere at three times: 1 day after explosion, at 20 days after the explosion when the SN Ia is at its peak brightness, and at the time T_b its center reaches minimum impact b , for two different redshifts $z = 0.05$ and $z = 0.35$ (left and right panel respectively) for each lensing configuration i.e., for each column. The caustics are also shown for the two shear values 0.20 and 0.40 in the $z = 0.05$ panel and for shear value 0.63 in the $z = 0.35$ panel (the linear units are in Einstein ring radii r_E).

Fig. 4.—

Similar to Fig. 4, with $m_d = 1 M_\odot$, but with $\gamma = 0.0, 0.05$, and 0.20 for the left column and $\gamma = 0.0, 0.10$, and 0.15 for the right. For the *3rd row* on the right $\gamma = 0.15, 0.26 = 1.76 \times 0.15, 0.47 = 3.15 \times 0.15$. In the *4th row* left column the caustics are for $\gamma = 0.05$ and 0.20 in the left panel, and the same as in Fig. 4 for the right panel. For the right column shear values 0.10 and 0.15 in the $z = 0.05$ panel and for shear value 0.47 in the $z = 0.35$ panel. The 1 and 20 day photospheres are not distinguishable at the scale shown.

Fig. 5.—

Similar to Fig. 5, with $m_d = 10 M_\odot$.

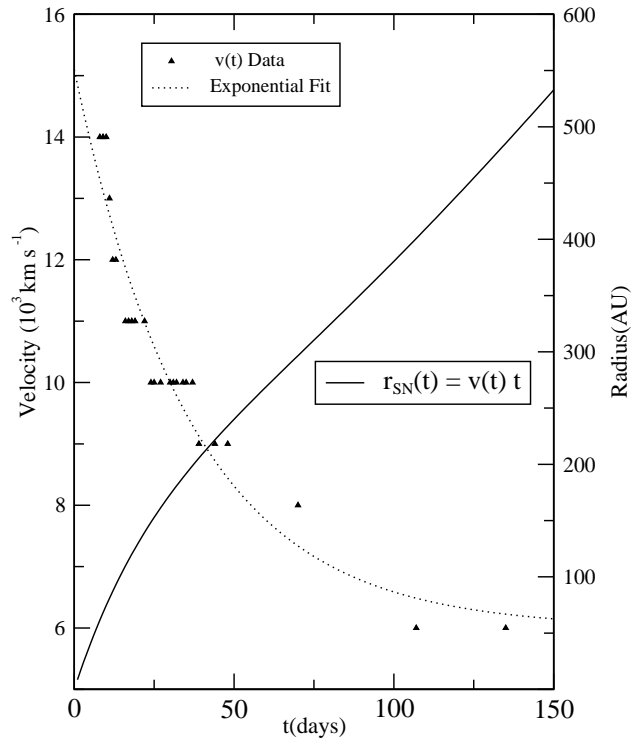


Figure 1

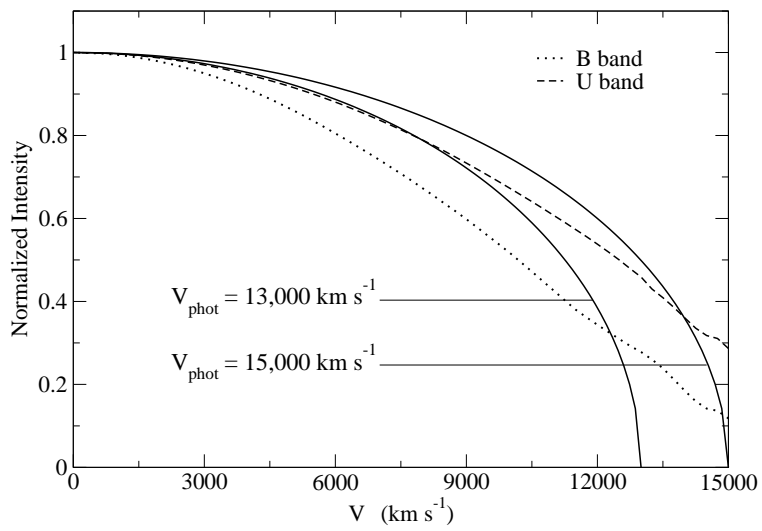


Figure 2

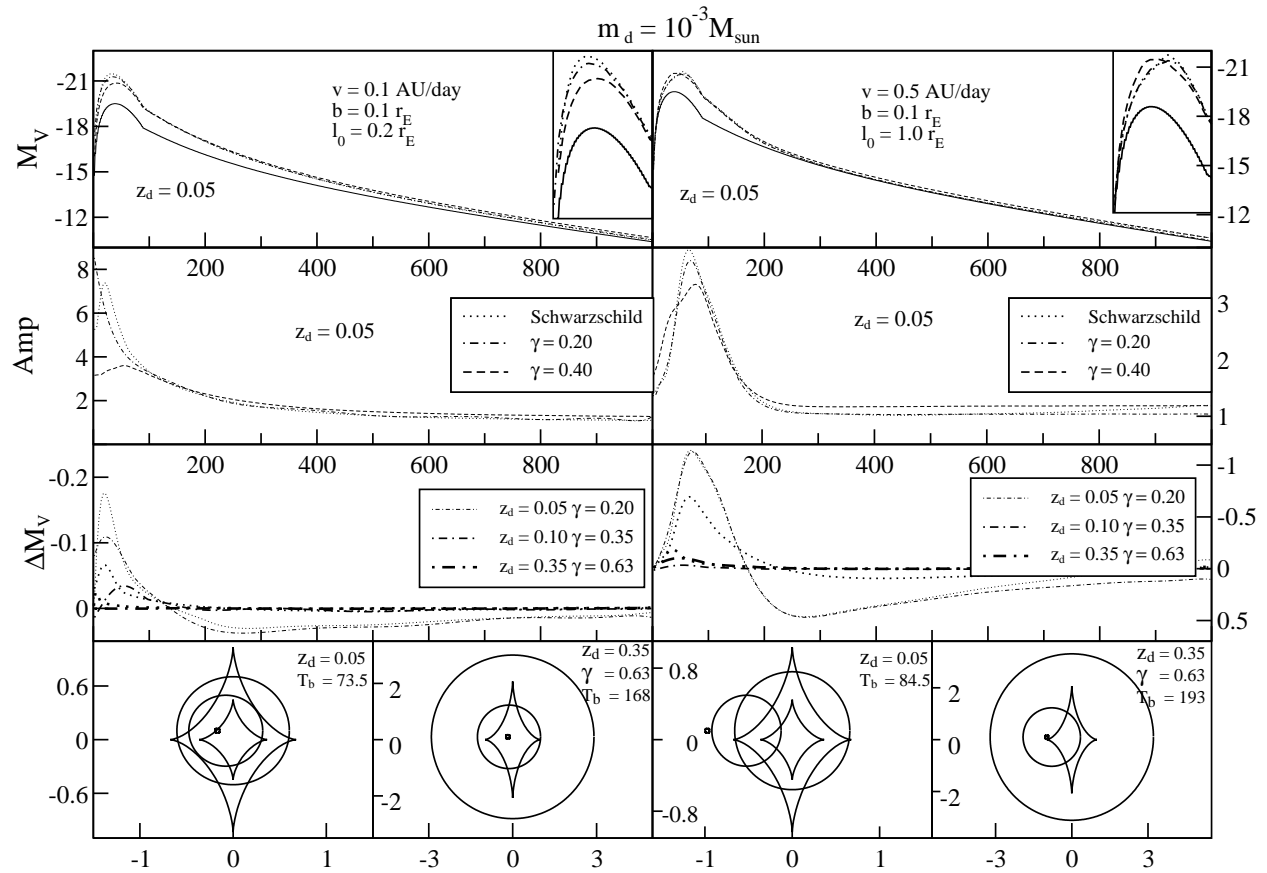


Figure 3

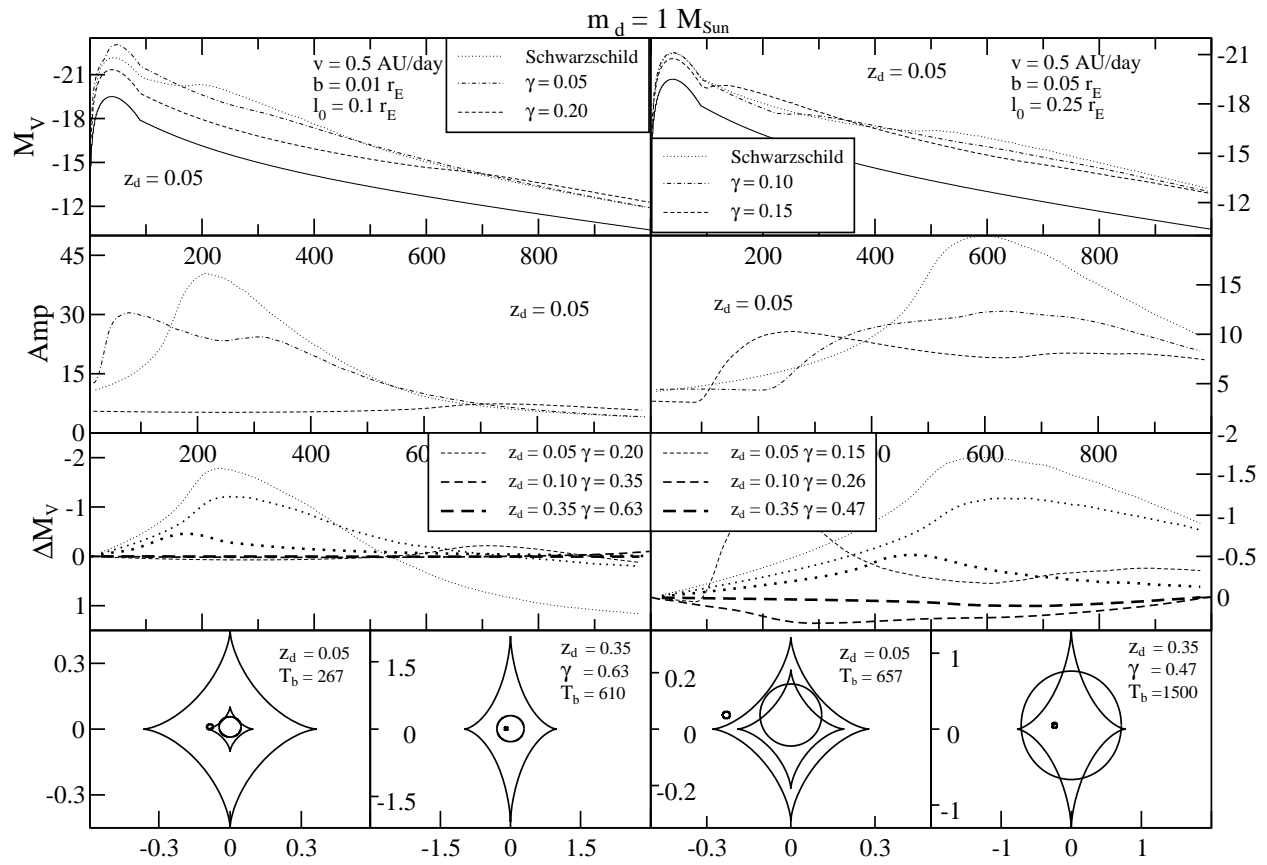


Figure 4

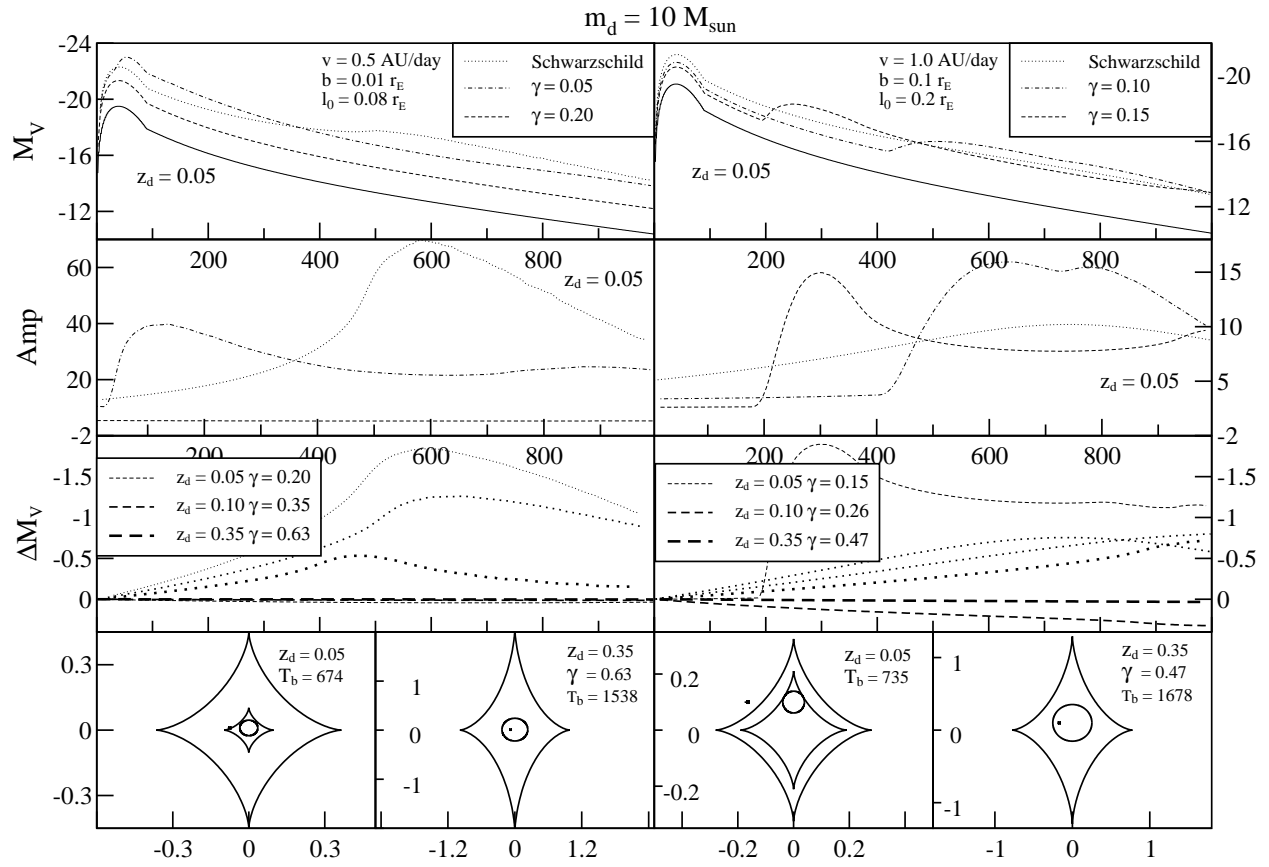


Figure 5